Effect of Humidity on the Ordering of PEO-Based Copolymer Thin Films

Joona Bang,[†] **Bumjoon J. Kim,**[‡,⊥] **Gila E. Stein,**[‡,⊥] **Thomas P. Russell,**[#] **Xuefa Li,**[○] **Jin Wang,**[○] **Edward J. Kramer,**[*,‡,§,⊥] **and Craig J. Hawker**[*,‡,§,||]

Department of Chemical and Biological Engineering, Korea University, Seoul 136-701, Republic of Korea, Materials Research Laboratory, University of California, Santa Barbara, California 93106, Department of Materials, University of California, Santa Barbara, California 93106, Department of Chemical Engineering, University of California, Santa Barbara, California 93106, Department of Chemistry and Biochemistry, University of California, Santa Barbara, California 93106, Department of Polymer Science and Engineering, University of Massachusetts, Amherst, Massachusetts 01003, and Advanced Photon Source, Argonne National Laboratory, Argonne, Illinois 60439

Received May 12, 2007; Revised Manuscript Received June 28, 2007

ABSTRACT: Solvent cast diblock and triblock copolymer films of poly(ethylene oxide-*b*-styrene) (PEO-*b*-PS) and poly(ethylene oxide-*b*-methyl methacrylate-*b*-styrene) (PEO-*b*-PMMA-*b*-PS), with cylindrical microdomains of PEO or PMMA−PEO, have a high degree of lateral ordering after solvent annealing. The relative humidity of the vapor during the solvent annealing has been shown to play an important role in achieving this order. After solvent annealing under high humidity a PEO-*b*-PMMA-*b*-PS triblock copolymer having a lamellar morphology in bulk develops a hexagonal array of depressed PEO domains on the film surface while the film surface remains flat under less humid conditions. Cross-sectional TEM and GISAXS show that the film annealed under high humidity conditions exhibits a well-defined hexagonally perforated lamellar (HPL) structure throughout its thickness, whereas a stack of lamellae aligned parallel to the surface is evident for films annealed at lower humidity. These results demonstrate the switchable nanoscopic structure of these films and strongly suggest that water vapor induces the morphological transition from lamellar to HPL by swelling the PEO domains.

Introduction

Producing nanostructured materials by self-assembly of block copolymers has been an active area of research for several decades[1,2] with significant theoretical and experimental effort devoted to understanding the phase behavior of block copolymers. Of recent interest has been the development of techniques and strategies that lead to the controlled orientation of these nanostructures as well as the identification of new morphologies.[1,2] Morphologies of A−B diblock copolymers in bulk include the "classical" phases of spheres, cylinders, gyroid, lamellae, and the metastable hexagonally perforated layer structure (HPL), depending on the block volume ratios.

Recently, thin films of block copolymer have attracted particular attention due to their potential applications in areas ranging from nanolithographic masks, high surface area catalyst supports, membranes, etc.[3–18] In these applications, critical issues are the control of both lateral ordering as well as the orientation of microstructures of block copolymers. A number of strategies have been developed to control the nanoscopic orientation of these thin films including surface modification using random copolymers,[19–21] manipulating the topology of the substrate,[22,23] applying external fields,[24–26] and using the

directionality imposed by solvent evaporation.[27–32] Of the five "classical" morphologies in block copolymers, most interest has been focused on spheres, cylinders, and lamellae, as they are more accessible using simple diblock copolymer systems. However, a limited number of studies on the ordering and the phase behavior of thin films having gyroid or HPL phase have been reported leading to nanostructures which offer added advantages when compared to traditional systems.[33–36]

In controlling the orientation and lateral ordering of microstructures in block copolymer thin films, one of the representative examples is poly(ethylene oxide)-containing block copolymers.[29–32] It was initially demonstrated that poly(ethylene oxide-*b*-styrene) (PEO-*b*-PS) diblock copolymers, having cylindrical microdomains of PEO, show a perpendicular orientation to the substrate with a high degree of lateral ordering. After solvent annealing, a defect-free lateral ordering was achieved over several micrometers. Although this system would be a fascinating candidate for the nanofabrication of addressable media, the PEO block is not readily removable by simple etching methods. To overcome this limitation, novel ABC triblock copolymers, poly(ethylene oxide-*b*-methyl methacrylate-*b*-styrene) (PEO-*b*-PMMA-*b*-PS) were recently developed and provide degradability via the PMMA middle block.[31] For these systems, it was shown that a high degree of lateral ordering could be achieved after solvent annealing and that a nanoporous structure is obtained by UV degradation of the PMMA block and simple aqueous washing.

In developing this system, it became apparent that processing conditions are critical to successfully aligning the nanoscopic template vertically and to order the resulting cylindrical pores over large surface areas. For these PEO-based systems, it was found that one of the most critical processing conditions was relative humidity during the solvent annealing step and it was

* Author for correspondence. E-mail: (E.J.K.) edkramer@mrl.ucsb.edu; (C.J.H.) hawker@mrl.ucsb.edu.
† Department of Chemical and Biological Engineering, Korea University.
‡ Materials Research Laboratory, University of California, Santa Barbara.
§ Department of Materials, University of California, Santa Barbara.
⊥ Department of Chemical Engineering, University of California, Santa Barbara.
|| Department of Chemistry and Biochemistry, University of California, Santa Barbara.
Department of Polymer Science and Engineering, University of Massachusetts, Amherst.
○ Advanced Photon Source, Argonne National Laboratory.

Figure 1. Schematic illustration of the solvent annealing chamber used in this study.

found that a high level of humidity ($>70\%$) is required to attain a high degree of lateral ordering.[31]

In this paper, a thorough investigation of the interplay between processing conditions (relative humidity) and triblock copolymer architecture in determining the morphology and orientation of PEO-*b*-PMMA-*b*-PS thin films is reported. With increasing relative humidity, the ordering of cylindrical microdomains was changed from parallel to perpendicular to the substrate. Remarkably, it was found that an increase in the relative humidity induces the formation of hexagonal PEO domain arrays in the surface lamella, and a morphological transition from lamellae to HPL structure throughout the film. The detailed morphologies of these films were characterized by scanning force microscopy (SFM), cross-sectional transmission electron microscopy (TEM), and grazing incidence small-angle X-ray scattering (GISAXS).

Experimental Section

Materials. ABC triblock copolymers, poly(ethylene oxide-*b*-methyl methacrylate-*b*-styrene) (PEO-*b*-PMMA-*b*-PS), were synthesized via reversible addition fragmentation transfer (RAFT) polymerization. The monomethoxy-terminated PEO was first modified with a dithioester group to give a PEO−RAFT macroinitiator, which was used to initiate the polymerization of MMA followed by styrene. Detailed procedures for the synthesis of the triblock copolymers are described elsewhere.[31] All polymers were fully characterized by ^{1}H nuclear magnetic resonance (NMR), using a Bruker 200 MHz spectrometer with the residual solvent signal as an internal reference. Size exclusion chromatography (SEC), using refractive index and photodiode array detectors (Waters) was employed to give the overall molecular weight and polydispersity.

Thin Film Preparation. The PEO-*b*-PMMA-*b*-PS triblock copolymers were spin-coated from benzene solutions onto silicon substrates. The film thickness, between 100 and 200 nm, was controlled by adjusting the solution concentration and spinning speed. The solvent annealing process was performed in a home-built glovebox chamber at room temperature, which is schematically illustrated in Figure 1. The whole glovebox chamber was continually flushed with humid air, which was produced by bubbling air through warm water ($\sim$50 °C). The relative humidity (R.H.) in the chamber was controlled by admixing dry air or adjusting the water temperature and was monitored just before the removal of the inner chamber. To investigate the effect of humidity on the ordering of triblock copolymer films, the R.H. in the solvent annealing chamber was adjusted from $\sim$50% to 90%. Once the desired R.H. condition was reached, it was maintained constant throughout the whole process. As shown in Figure 1, samples are placed in the much smaller sealed inner chamber, an upside down glass container on an larger glass Petrie dish, under saturated benzene vapor where the R.H. is initially the same as in the much larger outer chamber and annealed for 12 h, then the upside down glass container is simply removed from the Petri dish inside the much larger glovebox

that serves as the humidity chamber, thus allowing the benzene in the swollen sample to evaporate under a given R.H. condition.

Scanning Force Microscopy (SFM). To characterize the surface morphology of the triblock copolymer films, scanning force microscopy (SFM) height and phase images were obtained in the "tapping" mode using both a Digital Instruments Dimension 3100 and a Digital Instruments Nanoscope III.

Transmission Electron Microscopy (TEM). Cross-sectional TEM of the thin films was performed in order to investigate the detailed structure of the thin films annealed at high humidity. Samples for TEM study were prepared on Si substrates to provide identical conditions to those used to produce samples for SFM study. Samples were first stained under a saturated atmosphere of RuO_4 vapor in 0.5 wt % aqueous solution (Electron Microscopy Sciences) for 5−10 h to enhance the contrast between polymer phases. Diffusion of RuO_4 vapor into the PEO-*b*-PMMA-*b*-PS thin film provides the selective staining of PEO domain[37−39] as well as producing a 100−200 nm thick RuO_4 layer on the top of film, which protects the surface of polymeric film from the Ga ion beam of the focused ion beam (FIB) system operated at 30 kV. Cross-section samples for TEM were then prepared by a lift-off technique using a FEI DB235 dual-beam FIB system to produce a 120 nm thick film. It should be noted that a 1 μm thick Pt film was deposited on the polymer film before FIB milling to provide an extra protective layer on the polymer film. The morphology of PEO-*b*-PMMA-*b*-PS film was investigated by TEM using a FEI Tecnai G2 microscope operated at 200 kV.

Scanning Electron Microscopy (SEM). Field-emission scanning electron microscopy (SEM) was used to view the cross section of the block copolymer films. The fractured sections of the thin films were imaged using a JEOL 6300 SEM operated at 10 kV. Samples were stained under saturated RuO_4 vapor atmosphere over a 0.5 wt % aqueous solution of RuO_4 (Electron Microscopy Sciences) for 5−10 h to enhance the contrast between polymer phases.

Small-Angle X-ray Scattering (SAXS). To determine the bulk morphologies for triblock copolymers, small-angle X-ray scattering (SAXS) was performed using the beamline at the Materials Research Laboratory, University of California, Santa Barbara. Cu Kα X-rays ($\lambda = 1.54$ Å) are generated by a Rigaku rotating anode X-ray generator. The sample-to-detector distance was 1.7 m and the 2-D SAXS images were azimuthally averaged to produce one-dimensional profiles of intensity, I, vs wavevector, q.

Grazing-Incidence Small-Angle X-ray Scattering (GISAXS). The GISAXS measurements were conducted on the Sector 8-ID-E beamline at the Advanced Photon Source at Argonne National Laboratory. Monochromatic X-ray beams of 7.4 keV ($\lambda = 0.1675$ nm) were used. The sample-to-detector distance was 2285 mm, determined by calibration with a silver behenate standard ($d = 58.376$ Å). The incident angle was varied in 0.01 deg increments about the critical angle of the polystyrene matrix (0.16 deg), which produced controlled penetration depths ranging from 10 nm up to the full film thickness. The off-specular scattering at each angle was recorded with a 2D MAR−CCD detector. A lead beam stop
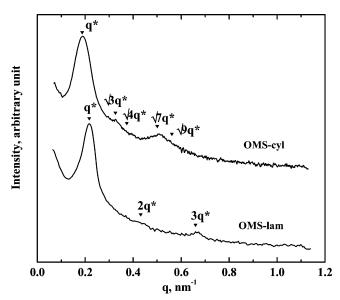
Figure 2. SAXS traces for PEO-*b*-PMMA-*b*-PS triblock copolymers. The filled triangles indicate the reflections at the marked q/q^* ratios of scattering vectors for cylindrical (OMS-cyl) and lamellar (OMS-lam) morphologies. Note that the SAXS trace of OMS-cyl is reproduced from ref 31. Copyright 2006 American Chemical Society.

Table 1. Sample Characteristics of PEO-*b*-PMMA-*b*-PS Triblock Copolymers

sample ID	M_{PS} (kDa)	M_{PMMA} (kDa)	M_{PEO} (kDa)	f_{PS}	f_{PMMA}	f_{PEO}	M_n/M_w
OMS-cyl	32.4	6.0	5.0	0.77	0.13	0.11	~1.1
OMS-lam	20.0	11.7	5.0	0.57	0.30	0.13	~1.1

blocked the strong specular reflection. Individual exposure times were 30 s, and 5–10 measurements at each angle were summed to provide a signal well above the background. Data were saved as 2048 × 2048 images in 16 bit TIFF format.

Results and Discussion

In previous work, the synthesis and characterization of ABC triblock copolymers, PEO-*b*-PMMA-*b*-PS, was developed and the block length for PMMA and PS was adjusted so that the bulk morphology shows PEO–PMMA cylinders in a PS matrix.[31] For these studies the RAFT polymerization strategy was further refined to allow accurate control over the length and weight percent of the PMMA and PS blocks by varying the reaction time and the conversion for each monomer. In this case, the block lengths of PMMA and PS were tuned so that a PEO/PMMA/PS lamellar morphology was obtained and the thin film behavior of these lamellar samples was compared with that of the previous PEO–PMMA core–shell cylinders. Table 1 lists two representative PEO-*b*-PMMA-*b*-PS (OMS) samples used in this study; OMS-cyl represents the sample showing the core/shell cylinders in the bulk, and OMS-lam designates the sample showing the lamellar morphology in the bulk. The bulk morphologies for each sample were investigated by SAXS experiments as shown in Figure 2. OMS-cyl clearly exhibits a cylindrical morphology, as evidenced by higher order reflections at q/q^* values of $1, \sqrt{3}, \sqrt{7}$, where q^* is the scattering vector of the first-order reflection. The expected reflections at the q/q^* value of $\sqrt{4}$ is probably missing because of the fact that the form factor has a minimum near this value. The absence of the reflection at $q/q^* = \sqrt{9}$ is due to the difficulty of resolving this weak reflection on the shoulder of the broad reflection at $q/q^* = \sqrt{7}$. For OMS-lam, the decreased PS volume fraction of 57% leads to a different morphology with reflections at $q = q^*, 2q^*$, and $3q^*$. This corresponds to a morphology with

lamellar periodicity but there is not sufficient information from the three SAXS reflections to determine whether this morphology consists of stacks of separate O, M, and S lamellae or whether O and M are mixed in a single lamella. However, it was shown previously a molecular weight of the PMMA block should be as large or greater than ∼ 5000 g/mol to form a separate domain, when the molecular weight of PEO block is 5000 g/mol. In this regard, it is believed that the PEO and PMMA domains in OMS-lam should be separate domains, especially in high humidity conditions since water is a nonsolvent for PMMA but a good solvent for PEO.

To investigate the thin film behavior of both cylindrical and lamellar samples, solutions were spin-coated onto silicon substrates and the film thickness was controlled between 100 and 200 nm by changing the solution concentration and the spinning speed. The films were then annealed under saturated benzene vapor for at least 12 h, while the relative humidity in the inner chamber before, and in the outer chamber, after annealing was controlled as desired. This humidity condition was observed to be critical for obtaining perpendicular orientation with a good lateral ordering for nanostructures formed from PEO-*b*-PS and PEO-*b*-PMMA-*b*-PS copolymers. At relative humidity (R.H.) of between 70 and 90%, excellent ordering and orientation was obtained and for simplicity, the humidity condition of R.H. ∼70–90% is subsequently referred to as "high R.H.", and that between 50 and 70% R.H. is referred to as "low R.H.". In this work, two samples, OMS-cyl and OMS-lam, were annealed under the saturated benzene conditions with the humidity controlled to be either "high R.H." or "low R.H.". All other conditions were kept the same.

Scanning force microscopy (SFM) was used to investigate the surface morphology of the thin films before and after annealing. Figure 3 shows the SFM phase images of OMS-cyl and OMS-lam on silicon substrates after annealing at either "low R.H." or "high R.H.". For OMS-cyl, the effect of humidity is very clear. At low R.H., the cylinders orient parallel to the substrate (Figure 3a), while at high R.H. perpendicular orientation of the cylindrical microdomains with good lateral ordering is observed (Figure 3b). At the intermediate relative humidity of 70% a mixed orientation, containing both parallel and perpendicular cylinders, is obtained. The most striking observation is however the strong dependence of the surface morphologies of OMS-lam films on relative humidity. At low R.H., the SFM height and phase images indicate a flat surface (Figure 3c), implying that the lamellae in the OMS-lam films are stacked parallel with respect to the substrate. At high R.H., the surface morphology of OMS-lam (Figure 3d) appears almost identical to that of the OMS-cyl annealed at high R.H., a surface morphology that can be described as a "hexagonally packed array" for both OMS-cyl and OMS-lam. This is surprising because no reorientation of lamellae can result in a hexagonally packed array of domains at the surface. In addition the 57 wt % polystyrene in the lamella forming sample makes it unlikely that the humidity is driving a lamellar-to-cylinder order–order transition by swelling the PEO containing block.

The observation that OMS-lam thin films annealed at high R.H. show a hexagonally packed array on the film surface—as with the OMS-cyl case—may provide a crucial key to understanding the mechanism of lateral ordering in PEO-based block copolymer thin films. This finding suggests that humidity plays an important role in driving the formation of ordered hexagonal arrays on the film surface. During the processing steps, the polymer films should initially be swollen with benzene vapor during annealing in the saturated benzene atmosphere. When
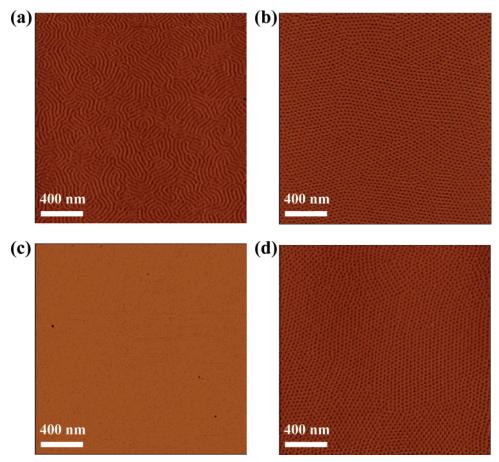
Figure 3. SFM phase images for PEO-*b*-PMMA-*b*-PS triblock copolymer thin films after annealing for 12 h in saturated benzene vapor under controlled humidity conditions. Key: (a and b) OMS-cyl annealed at low (<70%) and high humidity (>70%), respectively; (c and d) OMS-lam annealed at low and high humidity, respectively.

the films were removed under an atmosphere of controlled relative humidity, the solvent in the polymer film will evaporate from the top of the surface.[27,30] Cooling of the film surface will then occur and water will condense from the high relative humidity atmosphere and interact with the film surface. As the humidity in the atmosphere decreases, the amount of evaporative cooling necessary for condensation increases dramatically and at low enough R. H. the required temperature cannot be attained by evaporation of benzene. Decreasing the relative humidity from 90% to below 70% at an ambient temperature of 25 °C means that the dew point of the humid atmosphere decreases from 23 °C to below 19 °C. It is believed that the interaction between water and the hydrophilic PEO block in the polymer film may result in the hexagonal arrays and lead to long range ordering of the thin films. This hypothesis can be compared to the breath figure phenomenon, in which the water vapor interacts with the cooled surface of polymer films to induce hexagonal arrays of water droplets on the surface.[40,41] However, the size of arrays in breath figures is usually between 200 nm and several micrometers, 1−2 orders of magnitude larger than observed for the block copolymer domains above. While the mechanism may be different, the ability of humidity to produce hexagonal ordering of nanoscopic features of different materials is significant.

To understand the unusual morphological change for the OMS-lam thin films on going from low to high R.H., one possible explanation is that on increasing the humidity during processing the initial parallel lamella structures undergo a morphological transition to a hexagonally perforated layer (HPL) structure. Recently, the observation of HPL structures in thin films has been reported by Chang et al. for cylinder-forming

PS-*b*-PMMA diblock copolymers ($f_{PS} = 0.665$).[35] In this case, the HPL structure was likely due to the surface-induced reorganization, namely, the HPL structure was templated from the PMMA-wetted flat surface.

For the triblock copolymer films, the detailed internal structures of OMS-lam in Figure 3d were investigated by using cross-sectional TEM, SEM, and GISAXS measurements. Parts a and b of Figure 4 correspond to the cross-sectional SEM and TEM images for the OMS-lam annealed under high R.H. conditions, respectively. Although a hexagonal array pattern was observed on the surface, the cross-sectional SEM image of the fractured film clearly shows that six layers are stacked parallel to the substrate (Figure 4a). The contrast in this image is thought to arise from depolymerization of the PMMA in the electron beam. The detailed morphology is much clearer in the TEM image shown in Figure 4b. The sample was stained with RuO4, which is selective for PEO and PS, not for PMMA. Knowing that RuO4 is more selective for PEO than PS,[37−39] the staining time was adjusted to stain the PEO microdomains selectively. Therefore, the darker part in the image represents the PEO domains, and the lighter part corresponds to both PMMA and PS domains. From the TEM image, it can be seen that the thicker layers of PMMA and PS domains are perforated by PEO domains, forming the HPL structure as illustrated schematically in Figure 4c. Furthermore, all layers are well aligned parallel to the substrate over the entire film, and it is evident that the increase in the R.H. induces the morphological transition from the lamellar to the HPL structure for the lamellar forming PEO-*b*-PMMA-*b*-PS triblock copolymer film.

Since the cross-sectional TEM only reveals two-dimensional features, the three-dimensional nature of the films, such as the
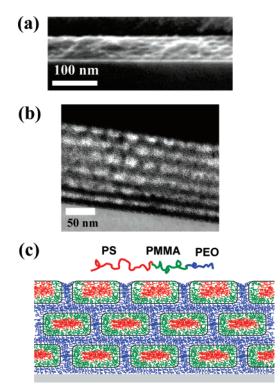
Figure 4. (a) SEM and (b) TEM images of the cross-section view of the film and (c) its schematic representation for OMS-lam annealed at high humidity (sample corresponding to Figure 3d).
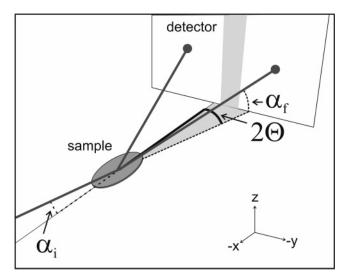

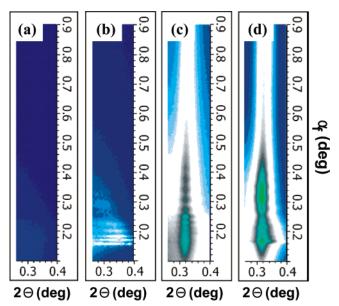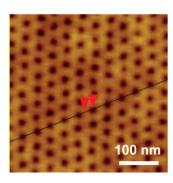**Figure 5.** Schematic of GISAXS geometry.

Figure 6. GISAXS pattern of OMS-lam at an incident angle of (a) 0.1° and (c) 0.17° of OMS-lam annealed at low humidity and (c) 0.1° and (c) 0.17° of OMS-lam annealed at high humidity.

stacking type of the hexagonal perforations in each layer, was further investigated by GISAXS experiments (Figure 5). The thin films were measured at incident angles above and below the critical angle of the OMS-lam films annealed under low R.H. and high R.H. conditions. Figure 6 presents the two-dimensional GISAXS patterns obtained for these samples. The horizontal axis is the in-plane diffraction angle 2θ, and the vertical axis is the out-of-plane diffraction angle α_f, as illustrated in Figure 5. For the OMS-lam annealed under low R.H. conditions, no diffraction peaks are observed when the incident angle is 0.1°, which is below the critical angle of the film (Figure 6a). This indicates that there is no lateral structure at the surface, which is consistent with SFM measurements. When the incident angle is 0.17°, the X-ray beam penetrates through the depth of the polymer film, and weak "streaks" are observed in the off-specular diffraction pattern along the α_f direction (Figure 6b).

These features are strongest in the range $0.16 < \alpha_f < 0.24$, i.e., between the critical angle of the polymer and the substrate, where standing waves inside the film amplify the scattering. (Bragg scattering from lamellar stacks would be observed at $2\theta = 0$, which is blocked by the beam stop.) We note a weak maximum in intensity near $2\theta = 0.35°$ ($q = 0.22$ nm^{-1}, $d = 27$ nm), consistent with the bulk lamellar spacing, and suggestive of some random orientation of the lamellae in the buried structure. Parts c and d of Figure 6 show the GISAXS patterns for the OMS-lam annealed at high R.H., collected at incident angles of 0.1 and 0.17°, respectively. Contrary to Figure 6a, a peak centered at $2\theta = 0.32°$ ($q^* = 0.21$ nm^{-1}) is observed in Figure 6c: This peak is sharp in 2θ-space, indicative of good lateral ordering, and nearly infinite along α_f, a signature of finite thickness on the order of 1 nm in the direction normal to the substrate.[42] Higher order reflections are observed at $\sqrt{3}q^*$ and $\sqrt{4}q^*$, consistent with the in-plane hexagonal packing observed in SFM measurements. The diffraction data in Figure 6d are similar to that shown in Figure 6c, except an additional peak is observed at $2\theta = 0.32°$ and $\alpha_f = 0.34°$, indicating both lateral and out-of-plane structure (a 3D lattice). Considering that these films are ~100 nm thick, the origin of the nearly infinite streaks along α_f is puzzling at first. However, SFM measurements under light tapping conditions demonstrate that the PEO microdomains at the free surface are actually depressed dimples ~2−4 nm deep (Figure 7). This is believed to result from the evaporation of water vapor from the PEO domain: During the solvent annealing process, the PEO domain is selectively swollen by water vapor, especially under high R.H. conditions. After the water evaporates, the PEO domain collapses and produces dimples at the free surface.

To confirm the *ABA* HPL structure demonstrated by the TEM measurements, the experimental patterns in Figure 6, parts c and d, were compared with simulations of the scattering using the distorted-wave Born approximation.[43] The perforations were modeled as short cylinders of PEO/PMMA (diameter:height = 20:10 nm) distributed in a PS matrix, with a nearest-neighbor periodicity of 34 nm and a vertical plane spacing (center-to-center distance between layers) of 14 nm. The divots at the free surface were modeled as 2 nm-deep cylindrical depressions, also with a diameter of 20 nm and a periodicity of 34 nm. (Note
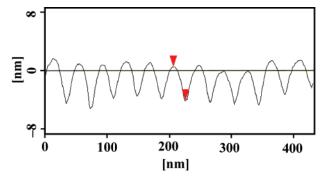
Figure 7. SFM height image for OMS-lam in Figure 3d and its height profile along the line on the SFM image.
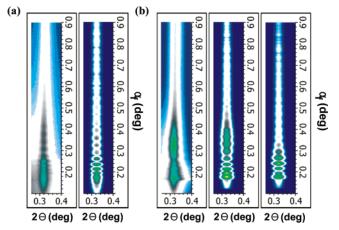

Figure 8. (a) GISAXS pattern (left) and its simulated pattern (right) at an incident angle of 0.1° for OMS-lam from Figure 3d. (b) GISAXS pattern (left) at an incident angle of 0.17° and its simulated pattern for *ABA* stacking (center) and the *ABC* stacking (right) for OMS-lam film shown in Figure 3d.

that the scattering power per unit volume from the depressions is approximately 100 times larger than the scattering power from the block copolymer microstructure.) As can be seen in Figure 8a, this simple model agrees with the experimental pattern collected below the critical angle. For comparison with the experimental data collected above the critical angle, the stacking sequence for the perforations was modeled as both *ABA* and *ABC*, which are both common in close-packed structures. The simulated scattering for *ABA* stacking closely matches the experimental pattern, as it accurately predicts the position of the out-of-plane Bragg peak at $\alpha_f = 0.34°$ (Figure 8b) while the simulated scattering from the *ABC* stacking is markedly different than what we observe experimentally.

The HPL phase of block copolymers in bulk has been extensively studied and the coexistence of *ABA* and *ABC* stacking is often observed.[37,39,44,45] It is also well-known that the free energy difference between the two different stackings is actually quite small,[46−48] and a small deformation can change the relative stability between these two stacking structures.[49] Park et al. reported a pure *ABC* stacking sequence for a HPL structure in poly(styrene-*b*-isoprene) (PS-*b*-PI) diblock copolymer thin films, which is contrary to our observations of *ABA* stacking. However, there are two differences between that PS-*b*-PI system and our PS-*b*-PMMA-*b*-PEO system: The PS-*b*-PI films were approximately 1 μm thick, and prepared by a thermal annealing process. Our PS-*b*-PMMA-*b*-PEO films were approximately 100 nm thick, and prepared by solvent annealing with a controlled humidity environment. In addition even in the bulk, morphologies are observed for "tricolor" triblock copolymers that are not seen in diblock copolymers.[50−53] Considering that *ABA* and *ABC* stacking sequences are nearly

degenerate in free energy,[54] different experimental conditions and different architecture (diblock vs triblock) could result in two different stacking structures.

Conclusion

The dramatic effect of processing conditions on the thin film behavior of cylinder and lamellar forming PEO-*b*-PMMA-*b*-PS triblock copolymers has been shown to result in different nanoscopic structures, not predicted by bulk studies. By changing the relative humidity during solvent annealing, both cylinders and lamellar morphologies which exhibited a parallel orientation to the substrate at low relative humidity (<70%) were observed to give the same hexagonal surface morphology with good lateral ordering at high relative humidity (70−90%). For the cylinders, this is simply a consequence of the perpendicular orientation of the PEO cylinders to the substrate surface. However for the bulk lamella materials, the hexagonal surface pattern results from a transition from a parallel lamellar to an orientated hexagonally perforated lamellar (HPL) structure. From the cross-sectional TEM and GISAXS experiments, it was confirmed that the actual structure throughout the film is the HPL and that PEO domains perforate the PS layers, and an *ABA* stacking of the perforation structure is suggested by the GISAXS analysis. As this morphological transition from lamellar to HPL structure is clearly induced by increasing the relative humidity, it is postulated that condensed water swells the PEO domains, leading to hexagonal ordering at the free surface. This hexagonal surface pattern then drives the formation of the HPL structure through the bulk of the film.

References and Notes

(1) Bates, F. S.; Fredrickson, G. H. *Annu. Rev. Phys. Chem.* **1990**, *41*, 525.
(2) Hamley, I. W. *The Physics of Block Copolymers*; Oxford University Press: New York, 1998.
(3) Hawker, C. J.; Wooley, K. L. *Science* **2005**, *309*, 1200.
(4) Hawker, C. J.; Russell, T. P. *MRS Bull.* **2005**, *30*, 952.
(5) Segalman, R. A. *Mater. Sci. Eng. R.* **2005**, *R48*, 191.
(6) Park, M.; Harrison, C.; Chaikin, P. M.; Register, R. A.; Adamson, D. H. *Science* **1997**, *276*, 1401.

(7) Templin, M.; Franck, A.; Du Chesne, A.; Leist, H.; Zhang, Y.; Ulrich, R.; Schadler, V.; Wiesner, U. *Science* **1997**, *278*, 1795.
(8) Spatz, J. P.; Herzog, T.; Moessmer, S.; Ziemann, P.; Moeller, M. *Adv. Mater.* **1999**, *11*, 149.
(9) Black, C. T.; Guarini, K. W.; Milkove, K. R.; Baker, S. M.; Russell, T. P.; Tuominen, M. T. *Appl. Phys. Lett.* **2001**, *79*, 409.
(10) Cheng, J. Y.; Ross, C. A.; Chan, V. Z. H.; Thomas, E. L.; Lammertink, R. G. H.; Vancso, G. J. *Adv. Mater.* **2001**, *13*, 1174.
(11) Lopes, W. A.; Jaeger, H. M. *Nature (London)* **2001**, *414*, 735.
(12) Kim, H.-C.; Jia, X.; Stafford, C. M.; Kim, D. H.; McCarthy, T. J.; Tuominen, M.; Hawker, C. J.; Russell, T. P. *Adv. Mater.* **2001**, *13*, 795.
(13) Cheng, J. Y.; Ross, C. A.; Thomas, E. L.; Smith, H. I.; Vancso, G. J. *Appl. Phys. Lett.* **2002**, *81*, 3657.
(14) Bal, M.; Ursache, A.; Tuominen, M. T.; Goldbach, J. T.; Russell, T. P. *Appl. Phys. Lett.* **2002**, *81*, 3479.
(15) Kim, D. H.; Kim, S. H.; Lavery, K.; Russell, T. P. *Nano Lett.* **2004**, *4*, 1841.
(16) Zhang, Q.; Xu, T.; Butterfield, D.; Misner, M. J.; Ryu, D. Y.; Emrick, T.; Russell, T. P. *Nano Lett.* **2005**, *5*, 357.
(17) Kim, B. J.; Bang, J.; Hawker, C. J.; Kramer, E. J. *Macromolecules* **2006**, *39*, 4108.
(18) Kim, B. J.; Chiu, J. J.; Yi, G.-R.; Pine, D. J.; Kramer, E. J. *Adv. Mater.* **2005**, *17*, 2618.
(19) Mansky, P.; Liu, Y.; Huang, E.; Russell, T. P.; Hawker, C. J. *Science* **1997**, *275*, 1458.
(20) Huang, E.; Pruzinsky, S.; Russell, T. P.; Mays, J.; Hawker, C. J. *Macromolecules* **1999**, *32*, 5299.
(21) Ryu, D. Y.; Shin, K.; Drockenmuller, E.; Hawker, C. J.; Russell, T. P. *Science* **2005**, *308*, 236.
(22) Segalman, R. A.; Yokoyama, H.; Kramer, E. J. *Adv. Mater.* **2001**, *13*, 1152.
(23) Kim, S. O.; Solak, H. H.; Stoykovich, M. P.; Ferrier, N. J.; de Pablo, J. J.; Nealey, P. F. *Nature (London)* **2003**, *424*, 411.
(24) Morkved, T. L.; Lu, M.; Urbas, A. M.; Ehrichs, E. E.; Jaeger, H. M.; Mansky, P.; Russell, T. P. *Science* **1996**, *273*, 931.
(25) Mansky, P.; DeRouchey, J.; Russell, T. P.; Mays, J.; Pitsikalis, M.; Morkved, T.; Jaeger, H. *Macromolecules* **1998**, *31*, 4399.
(26) Wang, J.-Y.; Xu, T.; Leiston-Belanger, J. M.; Gupta, S.; Russell, T. P. *Phys. Rev. Lett.* **2006**, 96, 128301/1.
(27) Kim, G.; Libera, M. *Macromolecules* **1998**, *31*, 2569.
(28) Kim, G.; Libera, M. *Macromolecules* **1998**, *31*, 2670.
(29) Kim, S. H.; Misner, M. J.; Russell, T. P. *Adv. Mater.* **2004**, *16*, 2119.
(30) Kim, S. H.; Misner, M. J.; Xu, T.; Kimura, M.; Russell, T. P. *Adv. Mater.* **2004**, *16*, 226.
(31) Bang, J.; Kim, S. H.; Drockenmuller, E.; Misner, M. J.; Russell, T. P.; Hawker, C. J. *J. Am. Chem. Soc.* **2006**, *128*, 7622.
(32) Kim, S. H.; Misner, M. J.; Yang, L.; Gang, O.; Ocko, B. M.; Russell, T. P. *Macromolecules* **2006**, *39*, 8473.
(33) Ludwigs, S.; Boeker, A.; Voronov, A.; Rehse, N.; Magerle, R.; Krausch, G. *Nat. Mater.* **2003**, *2*, 744.
(34) Park, I.; Lee, B.; Ryu, J.; Im, K.; Yoon, J.; Ree, M.; Chang, T. *Macromolecules* **2005**, *38*, 10532.
(35) Park, I.; Park, S.; Park, H.-W.; Chang, T.; Yang, H.; Ryu, C. Y. *Macromolecules* **2006**, *39*, 315.
(36) Lee, B.; Park, I.; Yoon, J.; Park, S.; Kim, J.; Kim, K.-W.; Chang, T.; Ree, M. *Macromolecules* **2005**, *38*, 4311.
(37) Zhu, L.; Huang, P.; Cheng, S. Z. D.; Ge, Q.; Quirk, R. P.; Thomas, E. L.; Lotz, B.; Wittmann, J.-C.; Hsiao, B. S.; Yeh, F.; Liu, L. *Phys. Rev. Lett.* **2001**, *86*, 6030.
(38) Zhu, L.; Cheng, S. Z. D.; Calhoun, B. H.; Ge, Q.; Quirk, R. P.; Thomas, E. L.; Hsiao, B. S.; Yeh, F.; Lotz, B. *Polymer* **2001**, *42*, 5829.
(39) Zhu, L.; Huang, P.; Chen, W. Y.; Weng, X.; Cheng, S. Z. D.; Ge, Q.; Quirk, R. P.; Senador, T.; Shaw, M. T.; Thomas, E. L.; Lotz, B.; Hsiao, B. S.; Yeh, F.; Liu, L. *Macromolecules* **2003**, *36*, 3180.
(40) Böker, A.; Lin, Y.; Chiapperini, K.; Horowitz, R.; Thompson, M.; Carreon, V.; Xu, T.; Abetz, C.; Skaff, H.; Dinsmore, A. D.; Russell, T. P. *Nat. Mater.* **2004**, *3*, 302.
(41) Srinivasarao, M.; Collings, D.; Philips, A.; Patel, S. *Science* **2001**, *292*, 79.
(42) In a bulk sample, the number of unit cells in each direction is effectively infinite, which produces sharp Bragg peaks in the diffraction pattern. In a thin film, the sample is infinite in-plane, but has a finite number of unit cells normal to the substrate. This produces "crystal truncation rods" in the diffraction pattern (diffraction "streaks" that are sharply peaked in 2θ space, but elongated in α_f). The length of the rods in α_f is inversely related to the thickness of film (of the unit cells) normal to the substrate. See ref 43 for more details.
(43) Stein, G. E.; Kramer, E. J.; Li, X.; Wang, J. *Macromolecules* **2007**, *40*, 2453.
(44) Ahn, J.-H.; Zin, W.-C. *Macromolecules* **2000**, *33*, 641.
(45) Loo, Y.-L.; Register, R. A.; Adamson, D. H.; Ryan, A. J. *Macromolecules* **2005**, *38*, 4947.
(46) Bolhuis, P. G.; Frenkel, D.; Mau, S.-C.; Huse, D. A. *Nature (London)* **1997**, *388*, 235.
(47) Bruce, A. D.; Wilding, N. B.; Ackland, G. J. *Phys. Rev. Lett.* **1997**, *79*, 3002.
(48) Pronk, S.; Frenkel, D. *J. Chem. Phys.* **1999**, *110*, 4589.
(49) Pronk, S.; Frenkel, D. *Phys. Rev. Lett.* **2003**, *90*, 255501/1.
(50) Breiner, U.; Krappe, U.; Abetz, V.; Stadler, R. *Macromol. Chem. Phys.* **1997**, *198*, 1051.
(51) Breiner, U.; Krappe, U.; Thomas, E. L.; Stadler, R. *Macromolecules* **1998**, *31*, 135.
(52) Chatterjee, J.; Jain, S.; Bates, F. S. *Macromolecules* **2007**, *40*, 2882.
(53) Epps, T. H., III; Cochran, E. W.; Bailey, T. S.; Waletzko, R. S.; Hardy, C. M.; Bates, F. S. *Macromolecules* **2004**, *37*, 8325.
(54) Matsen, M. W.; Bates, F. S. *Macromolecules* **1996**, *29*, 1091.

MA0710737